Single-molecule binding experiments on long time scales

Mark P. Elenko,[1] Jack W. Szostak,[2] and Antoine M. van Oijen[3,a)]
[1]*Program in Biological and Biomedical Sciences, Harvard Medical School, Boston, Massachusetts 02115, USA*
[2]*Howard Hughes Medical Institute and Center for Computational and Integrative Biology, Massachusetts General Hospital, Boston, Massachusetts 02114, USA*
[3]*Department of Biological Chemistry and Molecular Pharmacology, Harvard Medical School, Boston, Massachusetts 02115, USA*

(Received 21 April 2010; accepted 11 July 2010; published online 27 August 2010)

We describe an approach for performing single-molecule binding experiments on time scales from hours to days, allowing for the observation of slower kinetics than have been previously investigated by single-molecule techniques. Total internal reflection fluorescence microscopy is used to image the binding of labeled ligand to molecules specifically coupled to the surface of an optically transparent flow cell. Long-duration experiments are enabled by ensuring sufficient positional, chemical, thermal, and image stability. Principal components of this experimental stability include illumination timing, solution replacement, and chemical treatment of solution to reduce photodamage and photobleaching; and autofocusing to correct for spatial drift. © *2010 American Institute of Physics.* [doi:10.1063/1.3473936]

I. SINGLE-MOLECULE MICROSCOPY FOR BINDING

Binding is arguably the most fundamental of biomolecular interactions, and as such has been investigated using a wide array of methods. Canonical solution-phase methods are often limited to nonequilibrium measurements, are restricted in the rate and K_d ranges they can access, and provide only ensemble-averaged molecular information. As such, it can be challenging to capture the fine structure of molecular behavior with bulk-phase methods. We seek to take advantage of the blooming of single-molecule techniques that have already enabled the exploration of previously inaccessible biomolecular phenomena, including enzymatic memory, molecular motor motion, folding, conformational change, and catalysis.[1–4] The study of these phenomena at the ultimate level of sensitivity, that of a single molecule, allows for the observation of variations between and within single molecules under equilibrium conditions.

Single-molecule experiments have typically explored molecular interactions taking place at short time scales up to seconds or a few minutes. These typical time scales place a severe limit on the kinetic space that can be explored. For a diffusion-limited (10^8 M^{-1} s^{-1}) bimolecular interaction, a very tight K_d of 10 nM translates to an off rate of 1 s^{-1}, resulting in a duration of the binding cycle that is readily captured in a short time frame. Many bimolecular interactions of interest, however, display nondiffusion limited association rates or slower dissociation rates, resulting in binding cycle times which are orders of magnitude higher. We have developed a single-molecule approach that allows access to much longer time scales than previously possible, with the goal of capturing statistically significant numbers of events for molecules that bind with slow kinetics. The performance of this experimental system is illustrated by the study of artificially evolved RNA aptamers that bind a small-molecule ligand with slow kinetics.

We use total internal reflection fluorescence (TIRF) microscopy[5] to visualize receptor-ligand interactions at the single-molecule level. TIRF is a wide-field, multiplexed technique that allows for the observation of many molecules during an experiment. Using TIRF, only a thin (~100 nm) layer at the sample surface is illuminated, eliminating solution background fluorescence. Unlabeled receptor molecules are immobilized on a functionalized surface in a flow cell and are presented with a fluorescently labeled ligand in solution so that binding produces a fluorescent spot that goes dark again upon dissociation (Fig. 1). Recording the fluorescence intensity trajectories produced over time at each spot allows for the identification of on and off events, which can be used to calculate single-molecule rates and equilibrium constants, and analyzed for temporal dynamics and inter- and intramolecular heterogeneity.

To observe binding at slow kinetic regimes our approach allows us to extend experiments to time scales ranging from hours to days. Such unusually long runs are enabled by ensuring sufficient positional, chemical, thermal, and image stability. We discuss these requirements and the corresponding elements of the experimental approach in the sections below, followed by a description of representative demonstration experiments.

II. EXPERIMENTAL DESIGN

A. Single-molecule imaging

The basic prerequisites for long-term experiments are the same as for any single-molecule TIRF technique: immo-

a)Present address: Zernike Institute for Advanced Materials, Groningen University, The Netherlands. Author to whom correspondence should be addressed. Electronic mail: antoine_van_oijen@hms.harvard.edu.

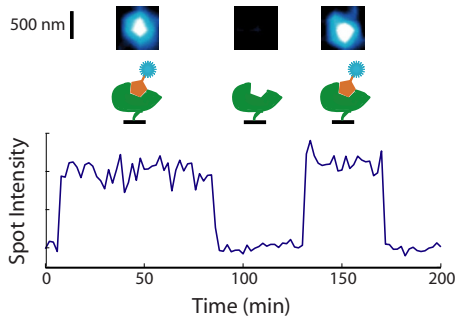

FIG. 1. (Color online) Single-molecule binding. The top row shows a single-molecule image from a RNA aptamer experiment (scale bar equals 500 nm), below which is a schematic illustrating the binding and unbinding of the fluorescently labeled ligand. At the bottom is the intensity trajectory for the single-molecule image from which the on- and off-event durations can be determined.

bilization of the receptor molecule and functionalization of the surface to deter nonspecific interactions with the labeled ligand. This immobilization is achieved by coupling silane molecules bearing amine groups to the surface of a glass microscope slip, providing a substrate for the covalent attachment of a layer of amine-reactive, high-molecular weight poly(ethylene glycol) (PEG) molecules[6] (for experimental details, see Sec. V). The high-density PEG layer on the glass surface serves to reduce nonspecific interactions between fluorescently labeled ligand and the surface. A small fraction of the PEG molecules are biotinylated on the end exposed to solution after surface coupling, so that streptavidin can be tightly bound to the top of the PEG layer. The receptor molecules of interest are also biotinylated so that they are captured at the surface by the streptavidin. The functionalized glass slips are integrated into sealed flow cells, with attached tubing allowing solutions to flow in and out.

Flow cells are placed on the stage of an inverted fluorescence microscope. For through-objective TIRF a high-numerical aperture objective is used both to illuminate the surface and collect the emitted fluorescence. The illumination is provided by a laser, and detection is done with a highly sensitive electron multiplying charge coupled device (EM-CCD) (Fig. 2). These elements, in conjunction with high-quality optical filters, enable the detection of labeled single molecules at the surface of the flow cell.

B. Positional stability

Positional stability is essential for long-duration microscopy. The depth of field of an optical system is determined by the diffraction limit in the direction along the optical axis and is given by $d=2\lambda\eta/(\mathrm{NA})^2$, where λ is the wavelength of the imaged light, η is the index of refraction for the immersion media, and NA is the numerical aperture. For the values used in the experiments described in this report ($\lambda=532$ nm, $\lambda=1.516$, and NA=1.45), the depth of field d is 767 nm. Absent any focal correction, mechanical drift will cause the image to go out of focus within minutes after the start of the experiment, thus necessitating an autofocusing mechanism. Lateral drift is also an issue as it must be assured that sequences of binding events can be correctly localized to the same molecule. Unlike focal drift, lateral drift can be

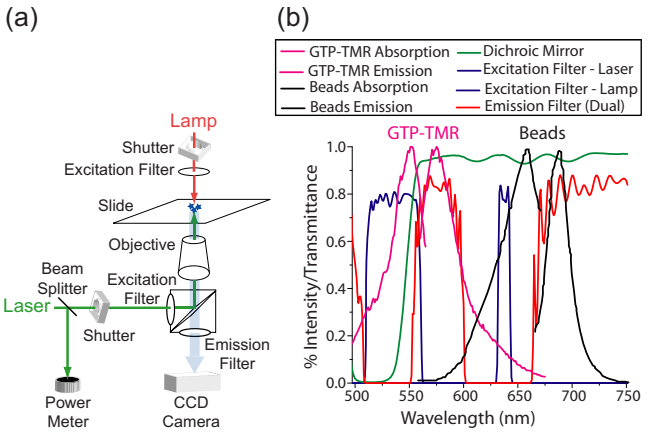

FIG. 2. (Color online) Imaging setup. (a) Both the laser used for single-molecule imaging and the lamp used for bead imaging during autofocusing are shuttered. The shutters, piezoelectric objective drive, and camera are controlled by software. (b) Spectra are shown for the separate laser and lamp excitation filters, the dichroic mirror, and the dual band emission filter, as well as for a labeled ligand used during the RNA aptamer experiments (GTP-TMR: guanosine triphosphate labeled with tetramethylrhodamine), and the reference beads.

factored out during image processing after an experiment. To address both focal and lateral drift we use fluorescent beads as fiduciary marks.

1. Focal stability

We have implemented an autofocusing technique that makes use of fluorescent reference beads, an approach originally pioneered by the Pollard group.[7] This technique is capable of preserving the focus over many days. Submicron (0.89 μm) fluorescent beads have been derivatized with biotin to adhere to the streptavidin-coated surface. A complication is that some receptor molecules (such as RNA aptamers), which are used at low concentrations (picomole range) in order to avoid overlap on the surface, can be nonspecifically adsorbed onto the beads and thus removed from solution and prevented from binding to the correct surface. Coupling the receptors to the surface before the beads are introduced solves this problem. The beads are excited by both the laser used to image the ligand label, and by a standard microscope lamp filtered at a wavelength that is not absorbed by the ligand label; both light sources are shuttered (Fig. 2). Such a configuration allows repetitive imaging of the beads without prematurely photobleaching the fluorescently labeled ligand molecules. The system performs autofocusing (Fig. 3) between single-ligand image acquisitions

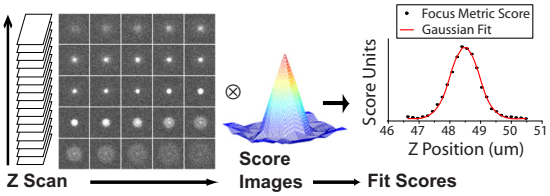

FIG. 3. (Color online) Autofocusing. (left) Autofocusing is performed by scanning through the z-axis while illuminating the beads alone. (center) Convolution with a "Mexican hat" edge/contrast detection kernel is used to compute a focus metric for scoring the images. (right) The resulting curve is fit with a Gaussian which yields the focus.

(that are obtained by laser illumination) by opening the lamp shutter and scanning through the z-axis using a piezoelectric objective drive (typically with step sizes of 160–320 nm) and recording an image at each step. These images, containing only the beads, are evaluated using a focus-score metric based on convolution with a contrast/edge detection kernel (a "Mexican hat"-type Laplacian of a Gaussian chosen to produce a good dynamic scoring range from the bead images)[8] [Eq. (1), where K_{xy} is the "Mexican hat" kernel shown in Fig. 3, I_{xy} is the image data, and m is a scaling factor]. The focus metric scores for the images at a number of positions along the z-axis (typically ~25) are fitted with a Gaussian, the center of which yields the current focal plane to which to move the objective [Fig. 3 (right)].

$$\text{Score} = \left[\frac{\Sigma_{x,y}(K_{xy} \otimes I_{xy})^2}{(\Sigma_{x,y} I_{xy})^2} \right] * 10^m. \quad (1)$$

Key parameters for this autofocusing protocol include the number of steps, the step size, and the delay between steps. The delay (60 ms) was chosen to avoid positional error induced by fast motion of the piezoelectric drive used with an objective that is coupled to the sample through viscous immersion oil. This delay time allows the sample-to-objective distance to equilibrate between position changes. As the autofocusing is currently done in software, the process is slower (just under 10 s when performing the 25 scan steps used for experiments described here) than would be dictated by the physical times and delays alone, leading to a potential tradeoff between the speed and accuracy of the autofocus. Given the low time resolution needed for the experiments, this extra amount of time needed for autofocusing did not pose any problems. Flowing in fresh solution can displace the surface by as much as a few micrometers; a total scan distance of 6–8 μm has been found to be sufficient for focus maintenance over many days and solution changes.

It is desirable to have several single beads within the field of view, and to avoid multibead aggregates which can incorrectly skew the calculations of the autofocusing routine. Because beads may be dislodged when solution is flowed in, an experiment should start with more than one bead in the field. We use bead solutions that consistently allow us to find fields of view with three to six single beads and no bead aggregates. For the bead density typically used, the focus scoring is linear with respect to the number of beads (Fig. 4).

The resolution of the autofocus system can be estimated by analyzing the mean square displacement (MSD) of the focus positions during single-molecule imaging runs (Fig. 5). The MSD as a function of time appears to be best fit by a diffusion-with-drift model in which the drift can be modeled as a monotonic physical change in the sample-to-objective distance. The y-intercept of the MSD function yields a value for the MSD at zero time and represents the square of the intrinsic focal resolution, which is found to be approximately 63 nm, about one twelfth of the depth of field (767 nm).

2. Lateral stability

The beads have the added benefit of serving as reference markers for factoring out lateral drift in the recorded movie. Even in the absence of jolts caused by flowing in solutions, the system experiences lateral drift of hundreds of nanometers on time scales of hours (Fig. 6). This drift corresponds to a potential error of multiple pixels, thus destroying the ability to effectively colocalize events to single receptor molecules. This drift is corrected by aligning all images using the bead positions, which can be found with subpixel accuracy using standard particle-finding algorithms (centroid or Gaussian). We use a set of MATLAB routines[9] to smooth the images and reduce background with a bandpass filter, locate peaks based on intensity thresholding and feature size (with an accuracy of a single pixel), and then find the centroids (with subpixel level accuracy).

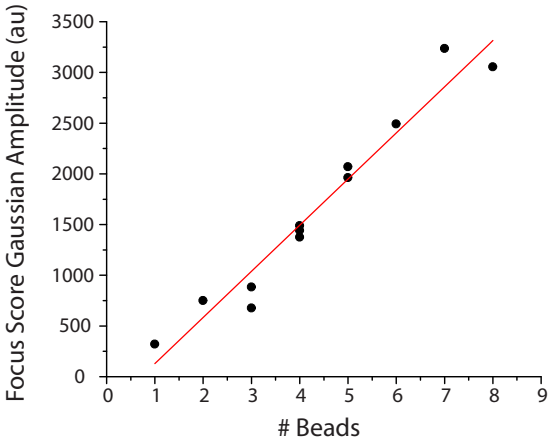

FIG. 4. (Color online) Autofocusing metric vs bead number. The amplitudes of the Gaussians that were fitted to the focus scores during autofocus z-scans (25 steps of 0.32 μm) are plotted with respect to the number of beads being used for focusing. Three to six beads are typically used for experiments.

C. Chemical stability

Long-term observation of individual ligand-receptor interactions requires two elements of chemical stability: The system must retain fluorescence viability over a time scale greater than the bound residence time for single events, and

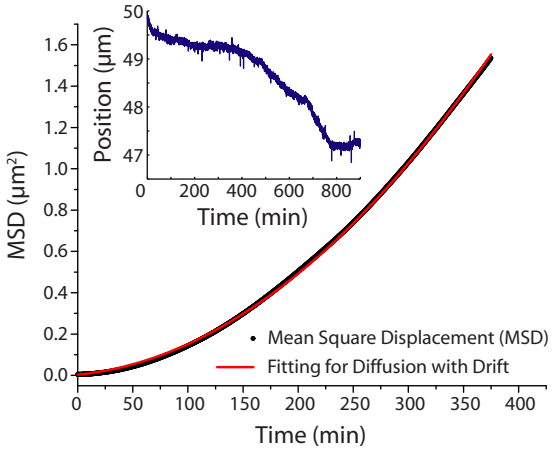

FIG. 5. (Color online) Long run position mean square displacement (MSD). The MSD is calculated from the focused positions (inset graph) for an autofocusing run with a 15 sec interval and no pumping. Data have been fit to an equation modeling a diffusion-with-drift process: $\text{MSD} = u^2t^2 + 2Dt + y0$, where t is the time, u (~3.1 nm/min) is the linear monotonic drift coefficient, D (~257 nm^2/min) is the diffusion coefficient, and the square root of the intercept y_0 (~63 nm) yields the intrinsic focal resolution.

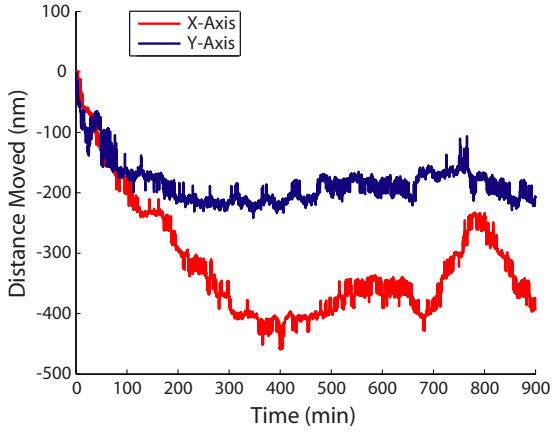

FIG. 6. (Color online) Lateral drift. The distance moved is based on the change in bead positions between images. Data shown are taken from a long run (the imaging interval is 15 s) without pumping to refresh solution.

retain binding competency over the lifetime of the experiment. The first requirement is addressed by minimizing photobleaching over the time scale being investigated, and the second is tied to the specific chemistry involved.

1. Fluorescence viability

The unbinding of a ligand cannot inherently be distinguished from the photobleaching of the fluorophore labeling the ligand. To ensure that the measurement of the duration of a binding event is not skewed by photobleaching that may occur before dissociation, the bleaching rate of the fluorophore should be at least an order of magnitude lower than the dissociation rate. The key to controlling the photobleaching lies in the fact that the photobleaching rate is determined by the number of absorbed photons and not the total time over which they are absorbed. Thus the fluorophore lifetime can be stretched over an arbitrary total real time by reducing the excitation intensity or, as described here, by imaging at intervals. This is done by capturing images in a noncontinuous manner, using a shutter on the laser (Fig. 7). The duration of the individual exposures is based solely on the minimum time required to achieve a viable signal with a sufficient signal-to-background ratio to accurately measure single-molecule intensities (here 200 ms). The interval duration determines the time resolution of the experiment. For the experiments described below, the shutter interval used was 2 min. Since reactive oxygen species are often responsible for photobleaching, an enzymatic oxygen scavenger system which removes molecular oxygen (O_2) from solution is frequently used to increase fluorophore lifetimes in single-molecule fluorescence experiments,[10] often in conjunction with an agent, such as the vitamin E analog Trolox, that can restore the advantageous triplet-state quenching provided by the O_2.[11,12] The effects of the various oxygen scavengers and related agents vary by fluorophore and chemical environment, so it is desirable to test the available possibilities with the experimental system being used. The oxygen scavenger of choice in the single-molecule fluorescence imaging field has traditionally been a combination of glucose oxidase and catalase, but the RNA aptamer case study described here used the newer protocatechuate-3,4-dioxygenase (PCD) system,[11,13] in combination with a Trolox triplet quencher, to ameliorate a problem with photodamage as discussed below.

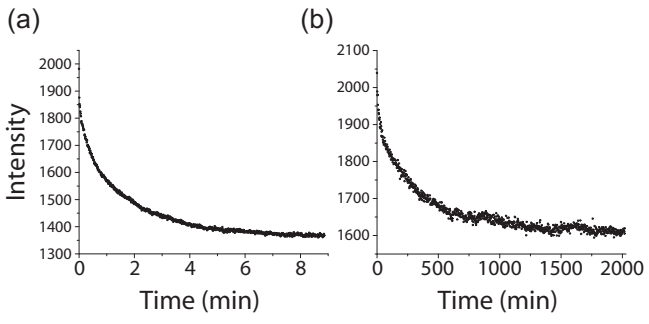

FIG. 7. Stretching of fluorophore lifetime. A fluorescently labeled DNA oligonucleotide (5′-biotin-GCG TAG ACT GAC TG-Cy3-3′) was immobilized at the surface and imaged to measure photobleaching. The rate of bleaching (a) ~0.66 min^{-1} is stretched out to (b) ~0.0032 min^{-1} by imaging at intervals (2 min) using a shutter. The intensities shown have had the camera's dark count subtracted (a) and (b), and been normalized to the laser power (b) only, as discussed in Sec. II F, to correct for long time scale laser fluctuation.

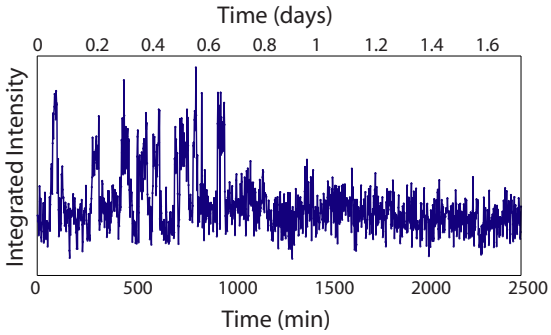

FIG. 8. (Color online) Loss of binding activity. The intensity trajectory for a RNA aptamer stops exhibiting binding despite the continued periodic addition of fresh solution. Such loss appears to be due to photodamage of the RNA.

2. Binding competency

The specific requirements for maintaining binding competency over a period of days depend, of course, on the specific molecules involved. For the system described in this report, the surface-immobilized receptor was a RNA aptamer and the ligand a small molecule (a fluorescently labeled nucleotide; see below). It was found that the RNA was susceptible to photodamage (Fig. 8), and that this problem could be reduced by the PCD/Trolox oxygen-scavenging system,[10] which doubled the half-time for particle loss. Such a scavenging system has a finite period of useful activity, thus the solution containing the labeled ligand and the scavenging system must be periodically refreshed (every ~3 h for the system described). Manual solution replacement has been done successfully, but is difficult over prolonged periods. A preferable alternative is the use of a larger, chilled (for enzymatic systems) reservoir of solution that can be pumped into the flow cell automatically at desired intervals. Flowing in additional solution has ramifications for positional and thermal stability (discussed elsewhere in this report).

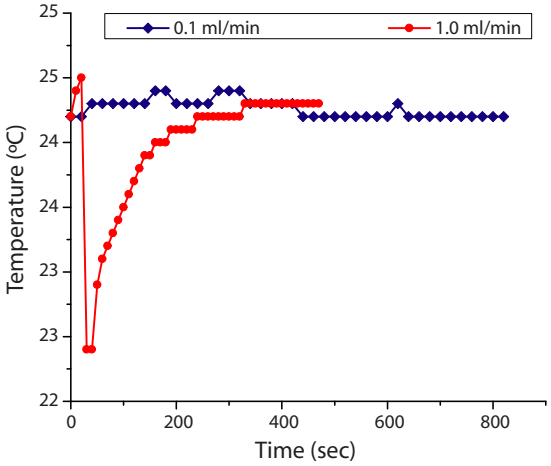

FIG. 9. (Color online) Pumping solution from a chilled (4 °C) reservoir. A flow cell with a temperature probe incorporated into the channel near the input port was used to monitor temperature recovery when flowing in solution from an ice-cold reservoir. Tubing length was ~60 cm and the volume flowed in was 0.55 ml.

D. Thermal stability

Most biochemical systems are temperature sensitive. In addition, maintenance of thermal stability is important to avoid inducing extraneous variation in the observed kinetics and, secondarily, for positional stability. The experimental setup is placed in a light-proof enclosure which contains several sources of heat, including the lamp. A fan integrated into the enclosure keeps the temperature within the flow cell stable within 0.2 °C. Flowing chilled solutions into the flow cell at a fast rate can result in a relatively large temperature perturbation which takes several minutes to equilibrate, a problem that can be avoided by using a slow flow rate (Fig. 9). Temperature fluctuations produce changes in the surface position, potentially causing loss of focus. This can be avoided by timing the autofocusing to occur just a few seconds before image acquisition and ensuring that the span of the *z*-scan is long enough to recapture the focus after a large fluctuation. Although it has not been found necessary for the experiments described here, a temperature control system (solution, stage, objective, or microscope based) can be used.

E. Surface integrity and stability

Coating surfaces with high-molecular weight PEG,[14] and the use of blocking reagents such as bovine serum albumin (BSA) are standard methods in the single-molecule field for minimizing nonspecific binding to the surface.[15] However, the resistance of these methods to nonspecific interactions has not been characterized at time scales longer than hours. The duration of such resistance to nonspecific binding depends on the molecular species being investigated and must be ascertained before long experiments are done. For the RNA aptamer system, long runs were performed without RNA and the number of nonspecific interactions of the labeled ligand (guanosine 5′-triphosphate coupled to tetramethylrhodamine) with the surface was evaluated at long (2 min) intervals and total periods (with and without automatic pumping of fresh solution) (Fig. 10), and at short intervals (500 ms). The average number of nonspecific fluorescent

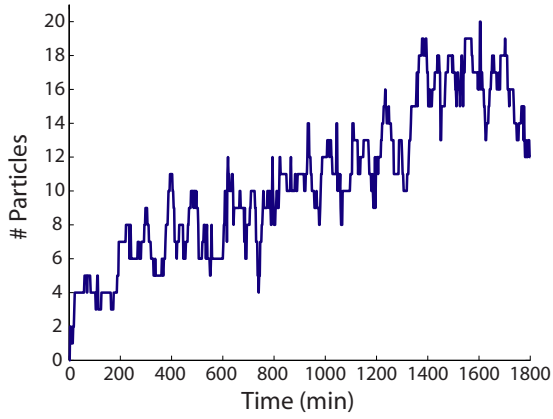

FIG. 10. (Color online) Nonspecific interaction with the surface. Data from 30 h of a run in which fresh labeled ligand (GTP-TMR) was pumped in every 3 h in the absence of the binding molecule (RNA aptamer). Data were smoothed with a moving median (window of 11 frames) to reduce noise.

spots per frame was in the range of 11–18, more than an order of magnitude lower than the number of spots seen for specific binding.

F. Stability of excitation intensity

Processing and analyzing the images captured with this system benefit substantially from an excitation intensity that is stable over the duration of the experiment. Large fluctuations in image intensity can significantly impact the thresholding needed to find spots and define events. By monitoring the output power of several solid-state lasers often used in the single-molecule community we found that laser warm-up time could take 1–2 h. More importantly, laser stability on the scale of hours to days can differ substantially between lasers, with one measurement of a laser model commonly used for short-duration single-molecule experiments showing a power drift of ~15% on the day scale and exhibiting occasional sharp jumps. When using a laser of unknown or low stability, the resulting movies should be checked for drift in excitation power as evidenced by changes in the overall brightness of the entire field of view. A beam splitter and a laser power meter (or a photodiode) can be added to the system to monitor laser power during experiments. Power data, or intensity data from an image region outside the illuminated area (thus capturing scattered light) that correlates with the laser power (Fig. 11), can be used to normalize fluorescence intensities over time.

III. GUANOSINE TRIPHOSPHATE-BINDING APTAMERS: A CASE STUDY

We illustrate the long time scale single-molecule imaging method described here with a study on RNA aptamers (see also Elenko *et al.*[16]). Aptamers are structured oligonucleotides that are capable of binding ligands with high specificity and affinity.[17] They can be produced by *in vitro* evolution but also have been found to occur naturally in riboswitch mRNAs.[18] For the experiments described here we used RNA aptamers to guanosine triphosphate (GTP), which were found by *in vitro* selection,[19–21] as the receptor molecules on the surface (see Sec. V for sequences). As ligand

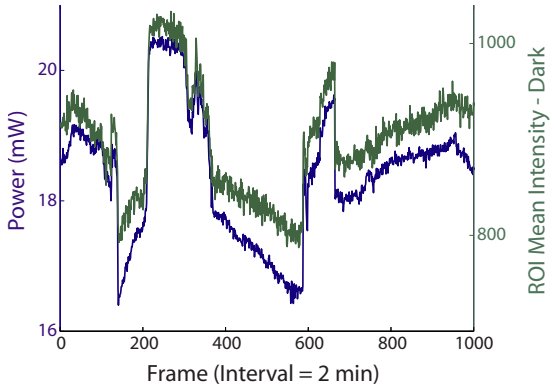

FIG. 11. (Color online) Image intensity correlates with laser power. Laser power (lower trace, left axis) was monitored during a run. The mean intensity of a corner region of the images outside the illumination area (with the camera dark count subtracted) was calculated (upper trace, right axis). Over a ~33 hour period, the correlation coefficient of the laser power and the image intensity was 0.98.

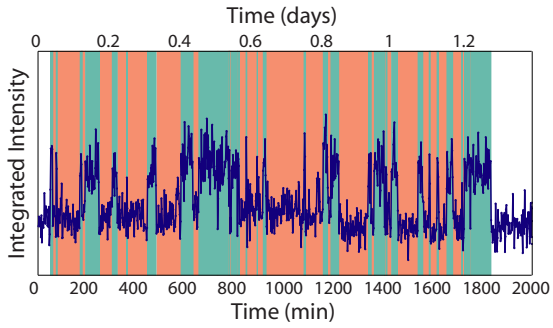

FIG. 12. (Color online) Long intensity trajectory from a RNA aptamer (class V M02) binding run. On and off events have been identified.

molecules we used GTP labeled with tetramethylrhodamine (TMR) (for experimental details, see Sec. V).

Several control experiments were performed to establish that the binding observed is the result of specific receptor-ligand interaction. Flowing in the labeled ligand (GTP-TMR) in the absence of aptamers on the surface does not result in apparent binding as compared to the binding observed when aptamers (9–4, 10–10, class V) are on the surface. Using an aptamer with a point mutation which renders it nonfunctional (9–4 M01) fails to produce binding. A different labeled ligand (uridine triphosphate-TMR) for which the aptamer on the surface (9–4) has no affinity also fails to show binding.

Given that the diameter of the streptavidin molecules which coat the surface is ~5 nm,[22] as compared to the ~224 nm diameter of a diffraction limited spot (for $\lambda = 532$ nm, NA=1.45), it is essential to find a receptor molecule concentration which sufficiently spaces the molecules out on the surface to spatially resolve individual molecules. The receptor molecule concentration must be determined empirically as the effective surface density depends not merely on the size, but the probability of capture at the surface and the fraction of active molecules. As an example, a 3 pM solution of fluorescently labeled short DNA oligonucleotide (5′-Biotin-GCG TAG ACT GAC TG-Cy3-3′), with a 20 min incubation time in the flow cell before flushing, produces a well spaced field with at most ~0.1 molecules per μm^2, checked by particle finding and single-step photobleaching. However, an 80 pM solution was used to similar effect for the class V RNA aptamer, and an 800 pM solution was used for the destabilized class V M02 mutant, which displays a tenfold reduced binding activity.

It is also necessary to establish the basic parameters for imaging. The first of these are the minimum laser power and image acquisition time (200 ms at ~17 W/cm^2) needed to achieve single-molecule detection. The photobleaching rate was measured by continuous imaging of the labeled ligand on plain glass slides (~0.045 s^{-1}). An initial estimate of the mean residence time was based on a bulk measurement of the off rate for the labeled ligand (0.044 min^{-1} for class V). This measurement was done by performing standard bulk fluorimetry for which the readout is the dequenching of the TMR upon binding of the GTP-TMR to the RNA, and the requenching upon disassociation. The rates were different from those for unlabeled ligand, an example of the issue that the label can perturb the interaction between the molecules. The interval between images (2 min) was chosen so that the photobleaching rate in real-time (rate constant ~220 min versus ~22 s under continuous illumination) was about an order of magnitude longer than the estimated mean residence time (~23 min for $t_{1/2}=1/k_{off}$). In cases in which it is not feasible to measure the off rate using a bulk assay one can iterate through imaging conditions for the single-molecule experiment until a viable interval is found.

Order-of-addition experiments showed that the aptamers had to be immobilized before the beads were added to the surface, as noted above. Based on experiments correlating the loss of aptamer activity (Fig. 8) with the laser illumination of the fluorophore, as opposed to the absolute time or other variables, it was concluded that the RNA was susceptible to photodamage. For example, if illumination was stopped for ~16 h after binding plateaued and then restarted, the number of active aptamers remained about the same, as opposed to a loss of activity for ~2/3 of the aptamers with the original illumination scheme. Illuminating in the presence of unlabeled GTP for ~16 h, followed by addition of labeled GTP-TMR produced a normal level of initial binding. The loss of activity appeared to be global within the flow cell and correlated with the interval between laser exposures. As noted previously, using a PCD/Trolox oxygen-scavenging system doubled the half-time for particle loss, increasing the length of the observed binding trajectories. These findings demonstrate that the extension of single-molecule observation schemes to time scales of many days may bring with it unforeseen photophysical consequences.

Our approach enabled the capture of particle intensity trajectories exhibiting multiple binding events over a long time scale (Fig. 12). The total number of events captured over all the aptamers of a given species was large enough (~400– ~1900) to allow a statistical analysis of the event-duration distributions. Both on- and off-time distributions can be fit accurately by single-exponential decay functions, indicating simple single-rate binding and dissociation kinetics [Fig. 13(a)]. On and off rate constants are consistent with values measured in solution-phase assays (for class V M02 the bulk off rate is ~0.023 min^{-1} versus ~0.044 min^{-1} and

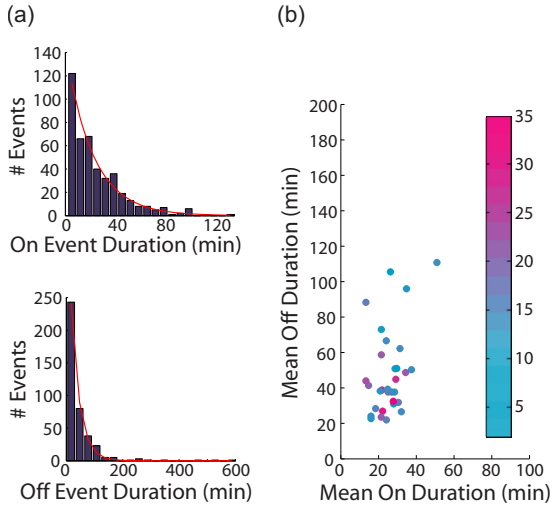

FIG. 13. (Color online) Event distributions and single-molecule kinetic space from a RNA aptamer (Class V M02) binding run. (a) On and off event distributions can be fit by single exponentials, corresponding to a single-rate binding process. (b) On and off event durations for each individual molecule can be averaged, allowing for a single-molecule plot of the kinetic space of the molecules in an experiment.

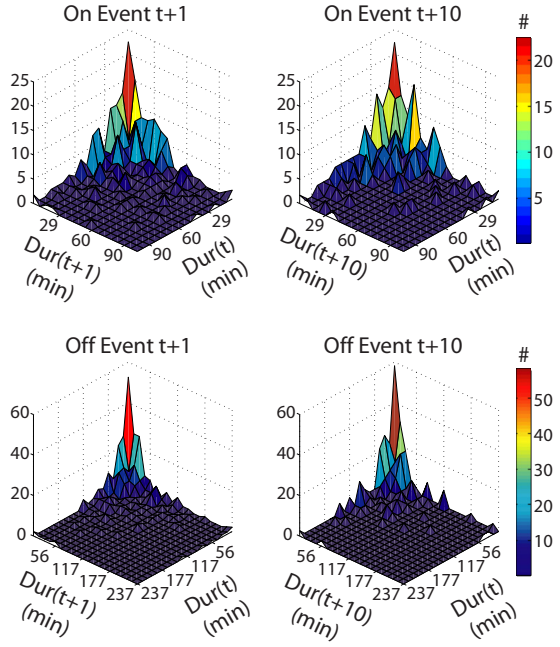

FIG. 14. (Color online) Event correlations. 2D histograms are shown for an aptamer (class V M02) binding run. On events (top row) and off events (bottom row) are binned to correlate the durations of every event t with event $t+1$ (left column) or with event $t+10$ (right column).

the bulk on rate is $\sim 0.024\ \text{min}^{-1}\ \text{nM}^{-1}$ versus $\sim 0.11\ \text{min}^{-1}\ \text{nM}^{-1}$). More significantly, meaningful single-molecule analysis was made possible by the presence of long event trajectories with many events. Such analysis includes the calculation of single-molecule K_d values by using the mean on and off event durations for each molecule to find single-molecule rates, and the use of these mean durations to localize individual molecules in a kinetic space useful for visualizing the kinetic structure of the population [Fig. 13(b)]. It was also possible to perform event correlations to examine the temporal dynamics of binding. For example, two-dimensional (2D) correlation histograms of event durations for every event and a following event imply that the aptamers do not have state memory of the sort seen with some protein enzymes,[23,24] as suggested by the absence of any diagonal feature (Fig. 14).

IV. FUTURE DIRECTIONS

We have demonstrated the feasibility of performing much longer single-molecule fluorescence experiments than reported before. Using readily available components it is possible to maintain the positional, chemical, thermal, surface, and image stability needed for single-molecule imaging on the time scale of days. Even though this experimental design allows the exploration of phenomena slower than have hitherto been investigated with single-molecule approaches, there is a significant caveat still to be addressed. Although TIRF has the advantage of reducing the background from solution fluorescence, in practice the actual concentration of labeled ligand that can be used is still quite low, typically $\leq \sim 1$ nM. Given the ligand concentration used for the RNA aptamer experiments (300 pM), the upper limit of experimental duration of a few days due to degradation caused by photodamage, and a simple threshold for the number of events required for trajectories to produce viable statistics, it is evident that only a small portion of kinetic space can be explored in detail, and that within that corner, the majority of possible equilibrium binding constants are not accessible (Fig. 15). There are many possible approaches to address this problem; we will briefly discuss four of them here: a load-bind-wash technique, two-color colocalization, a photoswitchable label, and zero-mode waveguides.

The simplest approach is to perform cycles of loading a high concentration of labeled ligand, incubating for a given interval to allow for binding, and then washing away the unbound ligand still present in solution before the actual image acquisition. This strategy clearly will alter the time resolution of the experiment. More problematically, just a few cycles of this procedure increases the number of molecules nonspecifically bound to the surface at any time by an order of magnitude (Fig. 16), a trend which continues as the num-

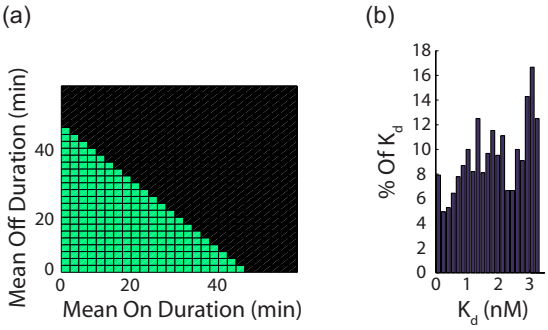

FIG. 15. (Color online) Accessible kinetic space for the RNA aptamer experiments. (a) To achieve a desired threshold number of events (20 events) given a viable total run time (48 h) and empirically representative degradation factor (0.35), the total possible binding cycle time (based on the on and off event durations) of the molecules is limited (green bins indicate combinations which exceed the threshold). (b) In this limited "kinetic space," only a small percentage of the possible K_d values are therefore accessible.

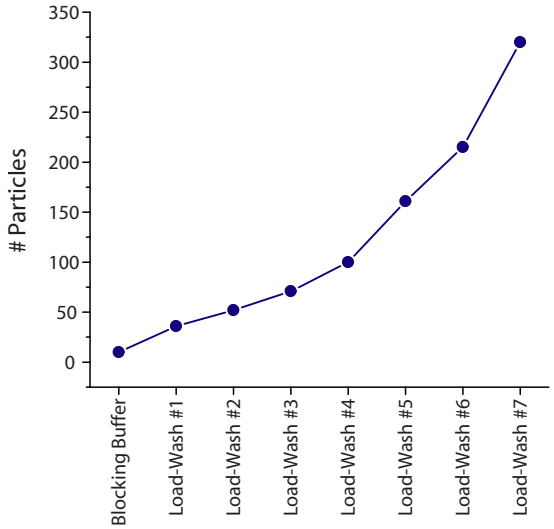

FIG. 16. (Color online) Buildup of nonspecifically bound particles during load-wash cycles. Labeled ligand (30 nM GTP-TMR) is added in the absence of RNA aptamers to quantify interaction with the surface. This run was performed with 30 μM ATP as one of a series of attempts to improve blocking.

ber of loading/washing cycle increases. Barring the development of better surface functionalization and blocking, this approach is unlikely to be viable.

The next simplest approach is to label both the immobilized receptor molecule and the ligand. The receptor molecules can then be colocalized with the bound ligand to a high degree of accuracy,[25,26] allowing nonspecific interactions in the vicinity to be distinguished from bona fide ligand-receptor interactions. This strategy also introduces a few complications. One label color could be used for both molecules but then the labels on the immobilized receptors must either be completely bleached before binding, possibly inducing photodamage, or they must be cleaved chemically or enzymatically, adding an additional layer of experimental complexity. In the case of two colors, one for the receptor and one for the ligand, interactions between the fluorophores must be assessed, as must photodamage. A seemingly logical step forward is to turn the described experimental design into a fluorescence resonance energy transfer (FRET) experiment. However, such a design would place a severe restriction on the possible time resolution. One premise of the current technique is that the lifetime of a label on the ligand is stretched to exceed the residence time of that ligand on the receptor. To perform FRET over at least tens of binding events requires that the lifetime of the receptor-coupled label be stretched to a much greater extent, increasing the minimum possible acquisition interval, and thus degrading the time resolution by at least an order of magnitude.

The remaining alternatives are technically more challenging. Photoswitchable fluorophores of the type used for new super-resolution microscopy methods[27] hold great promise for breaking the single-molecule concentration barrier. Activating such fluorophores in a TIRF geometry switches on those labels near the surface but labeled ligand that is not actually bound quickly diffuses away. Potential complications include the activation of nonspecifically bound molecules, and the need to work with the more complicated photophysics and resulting photochemistry which these labels incur. As a final strategy, zero-mode waveguides are subwavelength metal film nanostructures which preserve single-molecule detection while increasing the possible labeled ligand concentration by many orders of magnitude, up to the 100 μM range.[28] This design requires sophisticated fabrication, as well as more complicated detection and analysis, but should be compatible with the long time scale imaging techniques described here.

V. MATERIALS AND METHODS

For a schematic overview of the experimental setup, see Fig. 2. Through-objective (Olympus, 60× 1.45 NA, oil immersion) TIRF was done on an inverted microscope (Olympus IX71). The objective was driven by a piezoelectric drive (Physik Instrumente). The turret filter cube contained laser-quality excitation, dichroic, and emission filters (Chroma HQ535/50x, z532rdc, 51007m dual band and HQ545lp); the lamp condenser assembly was fitted with another emission filter (Chroma HQ 635/10x). A 532-nm solid-state laser (CrystaLaser) was used for single-molecule imaging, in conjunction with neutral density filters and other optics (Thor Laboratories). The laser and lamp were blocked by shutters (Ludl). An EM-CCD (Hamamatsu, cooled to −65 °C) was used for imaging. The entire system was in a light-shielding enclosure on a vibration-isolated optical table (TMC). Laser power during some experiments was monitored using a Coherent LabMax TO laser power meter with a Coherent PM3 detector. A syringe pump (Harvard Apparatus) was used to add or flush reagents. A LABVIEW (National Instruments) custom program was used to control the shutters, camera, piezoelectric drive, and pump.

Methods for slide functionalization and flow cell construction have been published.[29] Very briefly, glass coverslips were silanized with 3-aminopropyl triethoxysilane (Sigma), to which was coupled 5kD PEG with ~2% biotinylation (Nektar), coated with 1 mg/ml streptavidin (Sigma) and used to make single-channel flow cells with input and output tubing attached.

DNA oligonucleotides were purchased (IDT). RNA aptamer experiment details have been published.[16] The experiments described here made use of the 9–4, 10–10, and class V aptamers,[19,20] and mutants. RNA was prepared[20] with a 3′ A_{20} tail. The sequences for aptamers discussed here are (mutations in bold):

9–4: 5′-GG GAC GAG CAC GUG AAU CGA CUG CUU CGG CAG UGU CUC GAC GUG UGU AGG GGA AAG UAU CCC CCG UCC CAA AAA AAA AAA AAA AAA AAA-3′

9–4 M01: 5′-GG GAC GAG CAC GUG AAU CGA CUG CUU CGG CAG UGU CUC GAC GUG UGU AGG GGA **C**AG UAU CCC CCG UCC CAA AAA AAA AAA AAA AAA AAA-3′

10–10: 5′-GG GCT CAA CAG TAG CCA ACA CGA GTA CTG CTT CGG CAG TGG AAC CAA CGT AGT

ATG TTG AGC AAA AAA AAA AAA AAA AAA AA-3′

Class V: 5′-GG GGG CAU UUU GGU AGG UCG GUC GCU GCU UCG GCA GUG AGG GGU AGG CAU UGC UGG CCU AGG GUC CCC AAA AAA AAA AAA AAA AAA AA-3′

Class V M02: 5′-GG GGG CAU UUU GGU AGG UCG GUC GCU GCU UCG GCA GUG AGG GGU AGG CAU UGC UGG CCU AGG GU**U** **U**CC AAA AAA AAA AAA AAA AAA AA-3′

Briefly, the RNA was combined with a DNA dT_{20} 5′-biotinylated capture oligonucleotide (Roche), heated and cooled for folding and annealing, diluted in the aptamer buffer (with 0.1 mg/ml BSA, 0.001% Tween-20 added) and incubated in the flow cell for 20 min, followed by a buffer flush. Fluorescent carboxylated microspheres (0.89 μm Flash Red, Bangs Laboratories) coupled to biotinamidocaproyl-labeled BSA (Sigma) were incubated in the flow cell for 20 min and the cell was flushed. Guanosine-5′-[γ-thio]triphosphate (Sigma) was labeled with tetramethylrhodamine-5-iodoacetamide dihydroiodide (Molecular Probes/Invitrogen) to produce GTP-TMR. This coupling was verified by mass spectrometry (Bruker Esquire 3000 Plus and Bruker Esquire 6000). Thin layer chromatography was also used to verify that the product remained stable. The GTP-TMR was diluted to 300 pM using the previous buffer with the addition of oxygen scavenging system components: 50 nM protocatechuate 3,4-dioxygenase (Sigma), 2.5 mM 3,4-dihydroxybenzoic acid (protocatechuic acid) (Sigma), and 1 mM 6-hydroxy-2,5,7,8-tetramethylchroman-2-carboxylic acid (Trolox) (Sigma). This solution was refreshed in the flow cell every 3 to 3.5 h up to ten times. Fresh solution was either prepared and added manually or automatically pumped from a chilled reservoir.

ACKNOWLEDGMENTS

We thank Dr. Andrej Luptak for initial assistance, and Dr. Alonso Ricardo for assistance with compound characterization. J.W.S. is an investigator of the Howard Hughes Medical Institute.

[1] P. V. Cornish and T. Ha, ACS Chem. Biol. **2**, 53 (2007).
[2] N. G. Walter, C. Y. Huang, A. J. Manzo, and M. A. Sobhy, Nat. Methods **5**, 475 (2008).
[3] X. Zhuang, Annu. Rev. Biophys. **34**, 399 (2005).
[4] M. A. Ditzler, E. A. Aleman, D. Rueda, and N. G. Walter, Biopolymers **87**, 302 (2007).
[5] D. Axelrod, Methods Enzymol. **361**, 1 (2003).
[6] T. Ha, I. Rasnik, W. Cheng, H. P. Babcock, G. H. Gauss, T. M. Lohman, and S. Chu, Nature (London) **419**, 638 (2002).
[7] J. R. Kuhn and T. D. Pollard, Biophys. J. **88**, 1387 (2005).
[8] J. C. Russ, *The Image Processing Handbook* (CRC, Boca Raton, 2002).
[9] D. Blair and E. Dufresne, *The Matlab Particle Tracking Code Repository*, available at: http://physics.georgetown.edu/matlab/.
[10] C. E. Aitken, R. A. Marshall, and J. D. Puglisi, Biophys. J. **94**, 1826 (2008).
[11] I. Rasnik, S. A. McKinney, and T. Ha, Nat. Methods **3**, 891 (2006).
[12] T. Cordes, J. Vogelsang, and P. Tinnefeld, J. Am. Chem. Soc. **131**, 5018 (2009).
[13] P. V. Patil and D. P. Ballou, Anal. Biochem. **286**, 187 (2000).
[14] S. J. Sofia, V. V. Premnath, and E. W. Merrill, Macromolecules **31**, 5059 (1998).
[15] M. L. Visnapuu, D. Duzdevich, and E. C. Greene, Mol. Biosyst. **4**, 394 (2008).
[16] M. P. Elenko, J. W. Szostak, and A. M. van Oijen, J. Am. Chem. Soc. **131**, 9866 (2009).
[17] D. S. Wilson and J. W. Szostak, Annu. Rev. Biochem. **68**, 611 (1999).
[18] R. K. Montange and R. T. Batey, Annu. Rev. Biophys. **37**, 117 (2008).
[19] J. H. Davis and J. W. Szostak, Proc. Natl. Acad. Sci. U.S.A. **99**, 11616 (2002).
[20] J. M. Carothers, S. C. Oestreich, J. H. Davis, and J. W. Szostak, J. Am. Chem. Soc. **126**, 5130 (2004).
[21] J. M. Carothers, S. C. Oestreich, and J. W. Szostak, J. Am. Chem. Soc. **128**, 7929 (2006).
[22] W. A. Hendrickson, A. Pahler, J. L. Smith, Y. Satow, E. A. Merritt, and R. P. Phizackerley, Proc. Natl. Acad. Sci. U.S.A. **86**, 2190 (1989).
[23] H. P. Lu, L. Xun, and X. S. Xie, Science **282**, 1877 (1998).
[24] B. P. English, W. Min, A. M. van Oijen, K. T. Lee, G. Luo, H. Sun, B. J. Cherayil, S. C. Kou, and X. S. Xie, Nat. Chem. Biol. **2**, 87 (2006).
[25] G. J. Schutz, W. Trabesinger, and T. Schmidt, Biophys. J. **74**, 2223 (1998).
[26] A. Yildiz, J. N. Forkey, S. A. McKinney, T. Ha, Y. E. Goldman, and P. R. Selvin, Science **300**, 2061 (2003).
[27] M. Bates, B. Huang, and X. Zhuang, Curr. Opin. Chem. Biol. **12**, 505 (2008).
[28] M. J. Levene, J. Korlach, S. W. Turner, M. Foquet, H. G. Craighead, and W. W. Webb, Science **299**, 682 (2003).
[29] A. M. van Oijen, P. C. Blainey, D. J. Crampton, C. C. Richardson, T. Ellenberger, and X. S. Xie, Science **301**, 1235 (2003).